Structure of Molybdenum and Tungsten Sulfide $M_xS_y^+$ Clusters: Experiment and DFT Calculations

Melissa J. Patterson,[†] James M. Lightstone,[†,§] and Michael G. White*[,†,‡]

Department of Chemistry, Stony Brook University, Stony Brook, New York 11974, and Chemistry Department, Brookhaven National Laboratory, Upton, New York 11973

Received: August 15, 2008; Revised Manuscript Received: October 2, 2008

A combination of experiment and density functional theory was used to investigate the energetics of CO adsorption onto several small $M_xS_y^+$ (M = Mo, W; x/y = 2/6, 3/7, 5/7, 6/8) clusters as a probe of their atomic and electronic structure. Experimentally, tandem mass spectrometry was used to measure the relative yields of $M_xS_y^+(CO)_n$ cluster adducts formed by collisions between a beam of mass-selected $M_xS_y^+$ cluster ions and CO molecules in a high-pressure collision cell (hexapole ion guide). The most probable $M_xS_y^+(CO)_n$ adducts observed are those with $n \leq x$, that is, only one CO molecule bound to each metal site. The notable exception is the $M_5S_7^+$ cluster, for which the $n = 6$ adduct is found to have nearly the same intensity as the $n = x = 5$ adduct. Density fuctional calculations were used to search for the lowest energy structures of the bare $M_xS_y^+$ clusters and to obtain their relative stability for sequential CO binding. The calculated trends in CO binding energies were then compared to the experimental adduct distributions for assigning the ground-state structures. In this way, it was possible to distinguish between two nearly isoenergetic ground-state isomers for the $M_2S_6^+$ and $M_3S_7^+$ clusters, as only one isomer gave a calculated CO stabilization energy trend that was consistent with the experimental data. Similar comparisons of predicted and observed CO adsorption trends also provide evidence for assigning the ground-state structures of the $M_5S_7^+$ and $M_6S_8^+$ clusters. The latter contain metallic cores with most of the sulfur atoms bonded along the edges or in the faces of the metal core structure. The $n = 6$ and 7 adducts of $M_5S_7^+$ are predicted to be more stable than the $n = x = 5$ adduct, but only the $n = 6$ adduct is observed experimentally. The DFT calculations show that the $n = 7$ adduct undergoes internal bond breaking whereas the $n = 6$ framework is stable, albeit highly distorted. For the $M_6S_8^+$ cluster, the calculations predict that the two lowest energy isomers can bind more than six CO molecules without fragmentation; however, the apparent binding energy drops significantly for adducts with $n > 6$. In general, the ability of these small $M_xS_y^+$ clusters to bind more CO molecules than the number of metal atoms is a balance between the gain in CO adsorption energy versus the strain introduced into the cluster structure caused by CO crowding, the consequences of which can be fragmentation of the $M_xS_y^+(CO)_n$ cluster adduct ($n > x$).

Introduction

Transition metal sulfides such as MoS_2 and WS_2 have been the topic of much interest because of their ability to form well-organized cage structures on the nanoscale. Like carbon, the S−M−S layered structure of the metal sulfides has a high propensity for forming folded structures such as hollow nanotubes, nanoctahedra, and nanonions.[1−6] Metal sulfide nanomaterials also display a wide range of unique catalytic, photovoltaic, and lubricant properties.[7−9] For example, MS_2 nanotubes have shown potential as a hydrogen storage media,[10] whereas small MoS_2 nanoplatelets exhibit size-dependent band-gaps and are active photo-oxidation catalysts.[8] Small nanoplatelets of MoS_2 (1−5 nm) are also considered to be the active species in commercial hydrodesulfurization catalysts.[11] As the metal sulfide particles become very small, that is, molecular clusters, other structural motifs have been observed that are nonstoichiometric. These include the Mo_6S_8 moiety that contains an octahedral Mo_6 metallic core that is the building block of the Chevrel phase of MoS_2, for example, the superconducting AMo_6S_8 compounds (A = main group, transition, or lanthanide metal).[12,13] Crystalline Chevrel phases and amorphous ternary molybdenum sulfides have been found to be active catalysts for methanethiol synthesis and hydrodesulfurization.[14]

The observation of small cluster units in the condensed phase has given rise to a number of experimental[15−23] and theoretical studies[24−33] of isolated metal sulfide clusters as a function of size and metal-to-sulfur ratio. In the case of molybdenum and tungsten sulfide, gas-phase cluster techniques using laser ablation and sputtering sources have been used to generate M_xS_y clusters as neutral,[19] anion,[20,31] and cation[21] species with a wide range of stoichiometry. Experimental investigations are limited to probes of reactivity and electronic structure, whereas the atomic structures of the clusters are derived mainly from theoretical calculations using density functional theory (DFT). A few clusters have been observed as "magic" due to their large abundance in anion and cation cluster mass spectra and large HOMO−LUMO gaps as determined by anion photodetachment spectroscopy. One such species is the M_4S_6 cluster (M = Mo, W), which is prominent in both anion[20,31,34] and cation[35] cluster mass distributions with measured HOMO−LUMO gaps of ∼2

* Corresponding author. E-mail: mgwhite@bnl.gov.
† Stony Brook University.
‡ Brookhaven National Laboratory.
§ Present address: Naval Surface Warfare Center, Indian Head Division, Research, Development, Test and Evaluation, 4104 Evans Way Suite 102, Indian Head, MD 20640.

10.1021/jp807318c CCC: $40.75
Published on Web 11/04/2008

eV for the neutral cluster.[20] DFT calculations for the Mo_4S_6 cluster confirm its large HOMO−LUMO gap and predict a highly symmetric structure consisting of a Mo_4 tetrahedral core with the six sulfur atoms bridge bonded along the Mo−Mo edges.[20,21,31−34] The free Mo_6S_8 cluster with the "Chevrel" structure is also predicted to be a highly stable "magic" cluster with a relatively large HOMO−LUMO gap of 0.8−0.9 eV.[33,36] Murugan et al. used DFT to show that that the structurally related Mo_6S_{12} stoichiometric cluster has a similar HOMO−LUMO gap (0.7 eV) as well as large magnetic moment (4 μ_B).[32] A general conclusion of these DFT studies is that the small, gas-phase M_xS_y (M = Mo and W) clusters energetically favor 3D structures with metal−metal bonding cores. These structures can be contrasted to the platelet structures of larger, near-stoichiometric M_xS_y nanoclusters, which exhibit the same S−Mo−S layered structure of bulk MS_2. Nanoplatelets with sizes down to $Mo_{10}S_{24}$ have been recently observed in STM studies of self-assembled clusters on the surfaces of Au(111) and graphite.[37]

In the work reported here, we use the interaction of CO with mass-selected cluster beams to explore the structure of $M_xS_y^+$ (M = Mo, W) cation clusters. As demonstrated in a previous study of the $M_4S_6^+$ (M = Mo, W) magic cluster, a probe molecule such as CO or NH_3 preferentially binds to the exposed metal sites on the cluster. For these gas pick-up experiments, a beam of mass-selected $M_4S_6^+$ cluster cations is passed through a high-pressure collision cell containing the probe molecule (CO or NH_3) diluted in a He buffer gas. Mass analysis of the resulting cluster adducts, for example, $M_xS_y^+(CO)_n$, provides information on the number and relative stability of the M−CO binding sites. In the case of $M_4S_6^+(CO)_n$, the product mass spectra showed that the cluster binds up to four ($n = 4$) probe molecules with only a small amount of $n = 5$ adduct observable. DFT calculations of the total CO adsorption energies for the lowest energy $M_4S_6^+$ structure were consistent with the binding of only four CO molecules, beyond which the M−CO binding energy decreased dramatically. This combination of experiment and theoretical analysis provided further evidence for the highly symmetric structure of the $M_4S_6^+$ cluster.

As a follow up to our earlier work on the $M_4S_6^+$ cluster, we present a combined experimental and computational study of the structure and CO-adduct stability for the $M_2S_6^+$, $M_3S_7^+$, $M_5S_7^+$, and $M_6S_8^+$ clusters (M = Mo, W), which are the most prominent mass peaks in the $M_xS_y^+$ cation cluster distributions. In general, we find that the CO pick-up data are very sensitive to the individual metal−CO binding energies and can be used to distinguish between geometrical isomers that are predicted by DFT to have similar total energies. For the small, sulfur-rich $M_2S_6^+$ and $M_3S_7^+$ clusters, the experimentally favored geometries involve M−S−M bridge bonds and terminal sulfur bonds. The substoichiometric $M_5S_7^+$ and $M_6S_8^+$ clusters are predicted to have metallic cores consistent with trends found in earlier DFT studies. In addition to probing the relative isomer stabilities, the DFT calculations also illustrate the effects of multiple CO binding, which can induce structural changes and/or break bonds within the cluster framework as more CO molecules are added. The latter may have implications for using such clusters deposited on supports as catalysts for heterogeneous reactions under high-pressure (high coverage) conditions.

Experimental Section

The experimental work was performed on a cluster beam apparatus that uses a magnetron sputtering source (Oxford, NC200U) for generating gas-phase cation clusters.[38] The $M_xS_y^+$ clusters are formed by reactive sputtering of a metal target (Mo or W) with a mixture of 4% H_2S in Ar gas in a region containing high-pressure He gas (aggregation gas). Both the sputtering and the aggregation gases are introduced into the source using variable leak valves with typical backing pressures of 7.6 Torr (4% H_2S/Ar) and 22 Torr (He) for Mo-sulfide, and 7.9 Torr (4% H_2S/Ar) and 24 Torr (He) for W-sulfide. The magnetron was operated at a power of 185 W. The length of the high-pressure He region between the metal target and first exit aperture (cluster condensation region) for Mo-sulfide was 0.75 in. and 1.25 in. for W-sulfide.

The cluster ions leaving the source enter a quadrupole ion guide, which transmits them to a quadrupole mass filter. A single cluster mass is then selected by its mass-to-charge ratio and then focused into a hexapole ion-guide, which also houses a collision cell for the reaction of the cluster with different probe molecules. Mass spectra presented in this work were taken with the hexapole ion guide kept at ground potential, so that the relative ion−molecule collision energies mirrored the kinetic energy distribution of the incoming $M_xS_y^+$ ions ($\leq$2 eV in the laboratory frame). Gases of interest, in this case CO, are introduced into the collision cell using a variable leak valve with the pressure measured by a capacitance manometer (MKS). The CO sample was introduced as a mixture of 25% CO in He gas. The He gas collisionally cools the cluster adducts following the addition of CO molecules. Typical collision cell pressures for these experiments were in the range of 10−15 mTorr. The products were mass analyzed by a second quadrupole mass spectrometer and detected by a channeltron electron multiplier. All experiments were performed at room temperature.

Computational Details. The theoretical calculations were performed on the $M_xS_y^+$ clusters using all electron DFT with the DMol^3 code. A double numerical basis set with p- and d-polarization functions, comparable in accuracy to a Gaussian 6-31G** basis set, was used with a real-space cutoff of 4.9 Å. The generalized-gradient corrected approximation (GGA), with the Becke exchange plus Lee−Yang−Parr correlation (BLYP) functional, was used. The FINE quality standard was chosen for tolerances of energy, gradient, displacement, and self-consistent field convergence criteria of 1×10^{-5} au, 2×10^{-3} au/Å, 5×10^{-3} Å, and 1×10^{-6} au, respectively. The calculations were performed with spin state unrestricted. All of the cation isomers have a doublet state ($s = {}^1/_2$) as their final spin configuration with the exception of isomer I (C_{3v} symmetry) of the $M_3S_7^+$ cluster, which is a quartet ($s = {}^3/_2$). In the case of the highly symmetric $M_6S_8^+$ cluster (O_h), where degenerate orbitals can give rise to higher spin states, the low spin configuration ($s = {}^1/_2$) is calculated to be the lowest energy. Therefore, all of the clusters have a magnetic moment of 1 μ_B with the exception of the $M_3S_7^+$ cluster (isomer I), which is 3 μ_B. Relativistic effects were included in the calculations for the heavier tungsten atoms in the $W_xS_y^+$ clusters.[39]

Density functional calculations were also used to examine the bonding of CO with the $M_xS_y^+$ clusters. The total adsorption energy was defined relative to the energies of the bare cluster and the number of free CO molecules, that is,

$$E_{ads}(n) = E_{(cluster+nCO)} - [E_{cluster} + nE_{CO}] \quad (1)$$

where n is the number of CO molecules bound to the cluster, $E_{(cluster+nCO)}$ is the energy of the CO cluster adduct, $E_{cluster}$ is the energy of the free cluster cation, and E_{CO} is the energy of the free CO molecule. We also define the relative binding energy of a CO molecule to a cluster adduct as the change in total adsorption energies between adducts with one more adsorbate attached, that is,

$$\Delta E_{ads}(n) = E_{ads}(n) - E_{ads}(n-1) \quad (2)$$

Note that $\Delta E_{ads}(n)$ represents only an apparent CO binding energy as sequential CO addition can lead to structural changes that can significantly alter the stability of the cluster adduct. Hence, it is somewhat oversimplified to attribute the total energy difference between the n and $n-1$ adducts to the CO binding energy alone.

In general, the total energy for binding $n \times$ CO molecules depends on the specific metal locations of each of the CO molecules on the cluster, and only the lowest energy arrangements for sequential CO addition are presented in this work. For example, we searched for the lowest energy position of the first bound CO molecule to the $M_xS_y^+$ cluster ion, then searched for the lowest energy configuration among the remaining $x-1$ metal sites for the second CO molecule, and so on, until all of the metal sites are occupied. This approach is justified on the basis of the experimental evidence that multiple collisions with He gas are required to stabilize the internally "hot" adduct that results from CO addition. Simultaneous additions of CO are unlikely due to the large amount of internal energy (1−2 eV) that would be needed to be dissipated to prevent the CO molecules from simply boiling off the "hot" cluster adduct. Nonetheless, when the relative energies of different CO binding arrangements are small (<0.1 eV), multiple adduct structures may be possible. Although many of these were explored in this work, we limit the discussion to only those that represent the minimum energy path for sequential CO addition.

Structural isomers examined in this work were based on those obtained in previous studies of metal sulfide clusters. A combination of theoretical[32,33] and experimental studies in the gas phase,[31,40] solid state,[12,13] and solution phase[41−44] provided preliminary structures for M_xS_y clusters with similar or the same stoichiometry. Structures with no imaginary frequencies were considered valid, and those that had total energies within ~2 eV of the lowest energy structure were chosen for further calculations of CO binding. Optimized structures and total energies were generated for sequential nCO binding, and the energy trends were compared to the experimental CO adduct product distributions. Structural assignments were based primarily on the correct prediction of the CO "saturation" limit, that is, the point where the apparent CO binding energy for nCO molecules becomes positive or decreases appreciably relative to that of $(n-1)$CO (see eq 2). Except in the case of $Mo_6S_8^+$, the lowest energy isomers of the $M_xS_y^+$ clusters also yielded the best agreement with experimental trends in CO binding.

Results and Discussion

Figure 1 shows the mass spectra of the $M_xS_y^+$ (M = Mo, W) clusters produced by reactive sputtering. The mass spectra show "islands" of $M_xS_y^+$ clusters, each having the same number of metal atoms but different number of sulfur atoms. The most prominent mass peaks within each cluster island are considered to be the most stable and can be assigned to $M_xS_y^+$ clusters with an x/y stoichiometry of 2/6, 3/7, 4/6, 5/7, and 6/8. The $M_4S_6^+$ cluster is observed as the most prominent mass peak over a wide range of source conditions and is considered a "magic number" cluster of unusual stability. In a previous study of the $M_4S_6^+$ magic cluster, we showed that gas-phase pick-up experiments using probe molecules such as CO and NH_3 could be used to provide information on the number of exposed metal sites and the overall structure of the cluster.[21] Similar experiments using CO as the probe molecule are presented here for

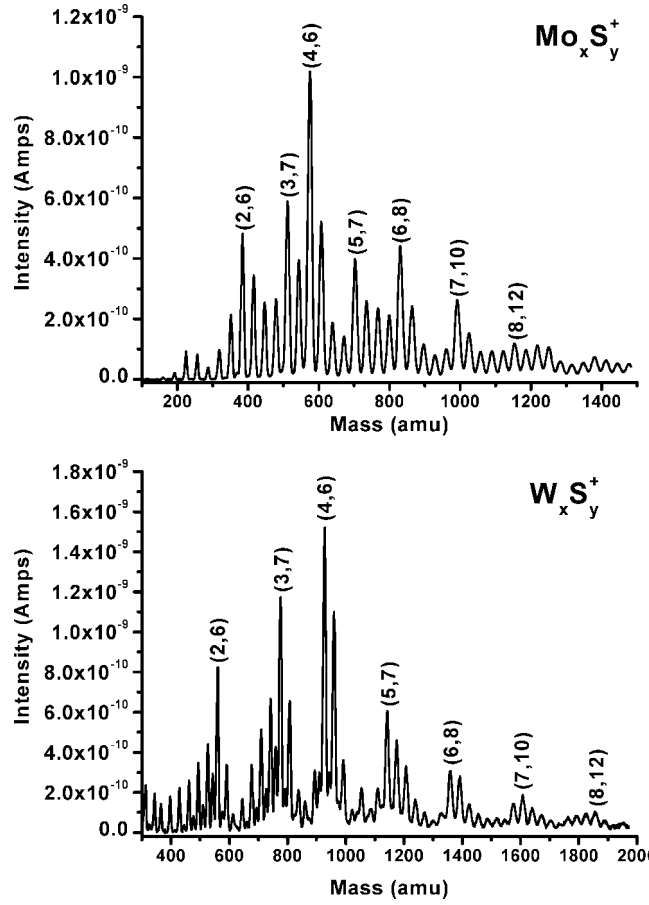

Figure 1. Mass spectra of $M_xS_y^+$cluster ions (M = Mo, W) produced in a magnetron sputtering source. Small peaks between the consecutive sulfur atom peaks in the $W_xS_y^+$ mass spectrum are a result of a small oxygen contamination.

the other prominent $M_xS_y^+$ clusters (M = Mo, W; x/y = 2/6, 3/7, 5/7, 6/8). The basic idea is that the observed mass distribution of the $M_xS_y^+(CO)_n$ cluster adducts is sensitive to the detailed structure of the cluster and its stability as CO molecules are added. More specifically, the adduct distributions can help identify the ground-state structure of the cluster from among the lowest energy isomers obtained by DFT geometry optimization. This is accomplished by comparing the observed adduct distribution with the calculated trends in total adsorption energies ($E_{ads}(n)$ in eq 1) for the different structural isomers.

The products observed from collisions of the cluster ions with CO correspond to simple cluster adducts in which CO adds molecularly, that is,

$$M_xS_y^+ + n\text{CO} \rightarrow M_xS_y^+(\text{CO})_n \quad (3)$$

Typically, the pressure of the He/CO gas inside of the collision cell was increased until the relative product yields were found to be approximately constant. Under these conditions, the most intense product masses are expected to correspond to the most thermodynamically stable CO adducts, with variations in reaction rates accounting for local minima or maxima in the adduct distributions. These assumptions are supported by previous ion beam studies of CO association reactions with metal cation clusters, where the most stable adducts (slowest reaction rates) are those that remain at higher CO/He pressures, especially the "saturated" adduct, which has the most CO molecules possible for a given cluster ion.[45−47] As seen below, most of the CO adduct product distributions observed in this

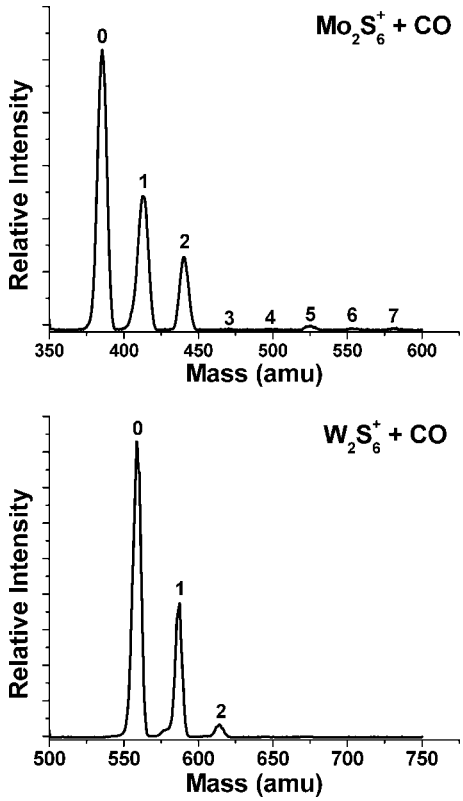

Figure 2. Mass spectra of products formed from collisions of the $M_2S_6^+$ (Mo, W) cluster with a 25% CO/He gas mixture.

work exhibit a distinct cutoff corresponding to the CO saturated cluster. It is the prediction of this CO saturation limit that is used to distinguish between structural isomers generated by DFT geometry optimizations.

As is common in transition metal complexes, the most stable orientation for CO binding to the Mo atom sites of these clusters is through the carbon atom. In this configuration, CO bonding involves charge transfer to the partially empty d-orbitals of the metal atoms through the CO 5σ orbital and back-donation of charge from the metal to the unoccupied CO 2π*orbital to relieve some of the built up negative charge.[48] Previous DFT studies on larger molybdenum sulfide clusters, for example, $Mo_{16}S_{32}$, show a binding energy of -0.95 eV[27] for CO on molybdenum, which is typical of the binding energies reported here.

$M_2S_6^+$ Cluster. The adducts formed by collisions between CO and the smallest prominent cluster, $M_2S_6^+$, are shown in Figure 2. For both Mo and W, adducts with one ($n = 1$) and two ($n = 2$) CO molecules are observed, although the bare cluster is the primary product at all pressures studied in this work. The latter suggests weak metal−CO binding and/or dissociation of the adducts before they can be detected by the downstream mass spectrometer. A low sticking probability could be the result of the small size of the cluster (fewer internal degrees of freedom), which makes it difficult to dissipate the energy of adsorption even with multiple collisions with the He background gas. In the case of $Mo_2S_6^+$, very small product peaks are also observed for $3 \leq n \leq 7$, whereas the product distribution for $W_2S_6^+$ falls off more rapidly above $n = 2$.

The two lowest energy structures calculated by DFT for $Mo_2S_6^+$ are shown in Figure 3. Isomer I consists of four bridging sulfur atoms between the Mo−Mo bond. The other two sulfur atoms are terminally bound to a single Mo atom. The Mo−Mo bond length is 2.82 Å, which is comparable to interatomic

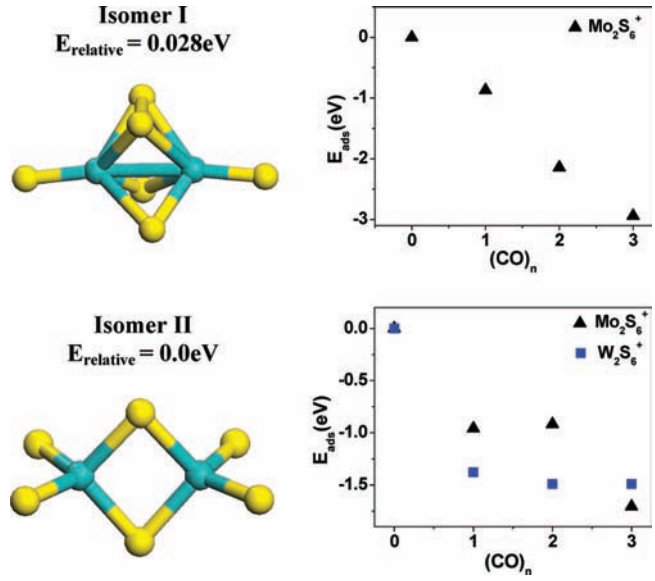

Figure 3. Optimized structures for the two lowest energy isomers of the $M_2S_6^+$ cluster (M = Mo, W). Figures adjacent to each isomer show the total adsorption energies for sequential adsorption of CO molecules to the $M_2S_6^+$ clusters as determined by DFT calculations.

distances and bond lengths of other Mo−Mo metal systems of the same stoichiometry.[33,41] The structure has near C_2 symmetry and is predicted to be only 28.0 meV higher in energy than the lowest energy structure, isomer II, also shown in Figure 3. Isomer II has near C_s symmetry with two bridging sulfur atoms connecting the two Mo atoms and four terminal sulfur atoms, two on each Mo atom. The isomer II structure was also found to be the lowest energy structure for the anion ($Mo_2S_6^-$) in the condensed and gas phases.[31,41] From the DFT calculations of Gemming et al., isomer II of Mo_2S_6 is expected to be the most stable among smaller Mo_2S_y clusters consistent with its large HOMO−LUMO gap (2.5 eV). These authors noted that the high stability of the isomer II structure of Mo_2S_6 could represent a structural motif for larger Mo_xS_y clusters or the bulk phase MoS_3.[31] DFT calculations by He et al. have found the same lowest energy structure for the $V_2S_6^+$ cluster.[40]

Alongside each of the calculated structures for $Mo_2S_6^+$ (I and II) in Figure 3 are plots of the calculated total adsorption energy for the sequential addition of CO. Despite being nearly isoenergetic, the two isomers exhibit very different CO adsorption behavior. Specifically, isomer I shows a nearly linear change in E_{ads} from $n = 1$ to $n = 3$, suggesting that adducts with three (or even more) CO molecules should be observable in pick-up experiments. This prediction disagrees with the observed $Mo_2S_6^+(CO)_n$ product distribution (Figure 2), which shows almost no $n = 3$ adduct. By comparison, the calculated CO adsorption energies for isomer II plateau at $n = 2$. A similar trend is found for the calculated $n = 1$ and $n = 2$ CO adsorption energies of isomer II of $W_2S_6^+$. For both metals, the calculated trend in CO binding energies for isomer II (see Table 1) suggests that the primary product is the $n = 1$ adduct, in agreement with the experimental product distributions (see Figure 2). The fact that the experimental $n = 2$ product yield is smaller, especially in the case of $W_2S_6^+$, indicates a small but nonzero binding energy for the second CO molecule. It is likely that the appearance of the $n = 2$ adduct depends sensitively on the second CO binding energy relative to the internal energy of the cluster; weakly bound CO molecules could be "desorbed" from the cluster before detection. The low probability for the $n = 2$ adduct means that larger adducts ($n \geq 3$) resulting from

TABLE 1: Calculated Binding Energies, $\Delta E_{ads}(n)$, for the Consecutive Addition of *n*CO Molecules to Isomer II of the $M_2S_6^+$ Cluster (M = Mo, W)[a]

n	$\Delta E_{ads}(n)$ $Mo_2S_6(CO)_n^+$	$\Delta E_{ads}(n)$ $W_2S_6(CO)_n^+$
1	−0.96	−1.38
2	+0.042	−0.11
3	−0.79	0.00

[a] All energies are given in eV.

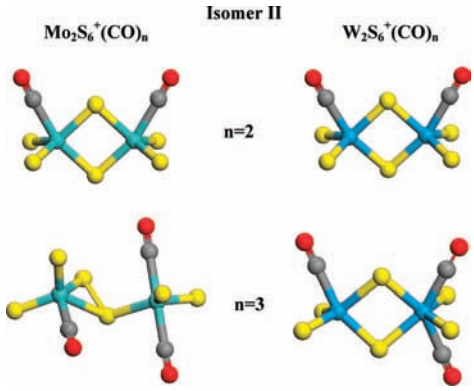

Figure 4. Geometry-optimized structures of the $n = 2$ and $n = 3$ CO adducts of isomer II of the $M_2S_6^+$ (M = Mo, W) clusters as determined from DFT calculations.

sequential addition are very unlikely, consistent with the observed product distributions. On the basis of these comparisons, the structure of the $M_2S_6^+$ (M = Mo, W) cluster is assigned to isomer II.

It is interesting to note that for isomer II of $Mo_2S_6^+$, the calculated CO binding energy for $n = 2$ is nearly zero, but dramatically increases again for $n = 3$ (see Table 1). By contrast, the CO binding energy for the $n = 3$ adduct of $W_2S_6^+$ (isomer II) is even smaller than $n = 2$. The difference in CO adsorption behavior can be more readily understood by viewing the optimized structures for the $n = 2$ and $n = 3$ adducts in Figure 4. It is seen that adding a third CO to $Mo_2S_6^+(CO)_2$ causes one of the Mo−S−Mo bridge bonds to break. This opening of the cluster framework is clearly energetically favored, but this species is likely to be a short-lived intermediate that undergoes further decomposition into smaller fragments. Any cation fragments resulting from dissociation would have masses well outside the range used to detect the cluster−CO adducts. By comparison, the $W_2S_6^+(CO)_3$ cluster remains intact, but the binding energy for the third CO molecule (see Table 1) is too small for the $n = 3$ adduct to be observed. As will be seen below, distortion or fragmentation of the cluster framework when the number of CO molecules exceeds the number of metal atoms is a general feature of these small $M_xS_y^+$ clusters.

$M_3S_7^+$ Cluster. The product mass spectra resulting from collisions between the $M_3S_7^+$ cluster with CO are shown in Figure 5. For both Mo and W, the most intense mass peaks correspond to CO adducts with $n \leq 3$, with the most probable product being $M_3S_7^+(CO)_2$. These observations are consistent with a cluster structure in which all three metal atoms are exposed and can bind CO, but with an overall stabilization energy that is a maximum for only two CO molecules ($n = 2$). Figure 6 shows the three lowest energy structures for the $M_3S_7^+$ clusters found by DFT geometry optimizations. Isomer I consists of a triangular metal core with two bridging sulfur atoms along each edge (total of 6). The seventh sulfur atom is face capped on one side of the metal triangle, and the cluster has an overall symmetry of C_{3v} (3-fold axis perpendicular to plane of page in

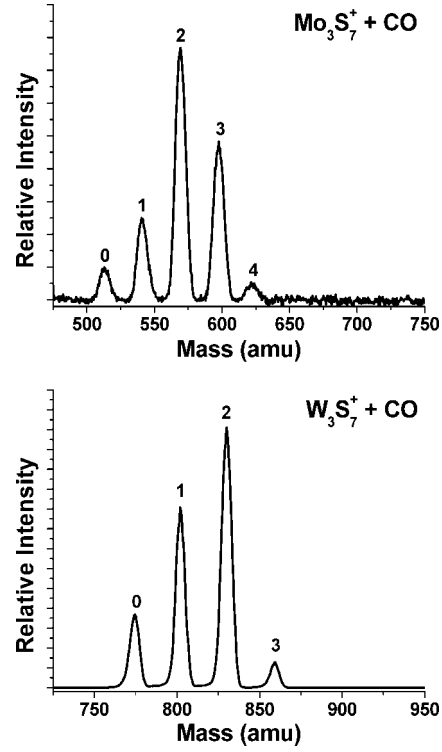

Figure 5. Mass spectra of products formed from collisions of the $M_3S_7^+$ (M = Mo, W) cluster with a 25% CO/He gas mixture.

Figure 6). Isomer I is thought to be the basic building block of a large number of compounds in the condensed phase such as $[NH_4]_2[Mo_3S_{13}]$[42,44] and the center of a trinuclear cluster complex with outer dithiolate ligands that has been identified as a novel molecular conductor.[43] Isomer II is structurally similar to I, but contains two face capping sulfur atoms and has a lower symmetry (C_1). The lowest energy structure, isomer III, has C_s symmetry with each metal atom bonded to one terminal sulfur atom, two bridging sulfur atoms, and one face capping sulfur atom. Note that isomers I and II contain a triangular M_3 metal core, whereas isomer III is predicted to have only one relatively long metal−metal bond (2.93 Å).

The structures for the cluster adducts, $M_3S_7(CO)_n^+$, were geometry optimized, and the total adsorption energies, $E_{ads}(n)$, were calculated for each of the three isomers. The computed trends in adsorption energies are shown in Figure 6. For isomer I, the total adsorption energy, $E_{ads}(n)$, steadily increases to $n = 6$, after which it reaches a plateau. The calculated adduct structures for $n \geq 6$ (not shown) exhibit significant structural distortions, which we attribute to steric effects associated with multiple CO binding to the metal atoms. The calculated adsorption energies for sequential CO addition to isomer II show similar behavior (Figure 6). For both isomers I and II, the calculated total adsorption energies predict that the $n = 6$ adduct should be observable, in clear disagreement with the experimental product mass spectra (Figure 5).

The calculated adsorption energies for isomer III show very different behavior for sequential CO binding (Figure 6). The calculated total adsorption energies for both Mo and W are seen to reach a plateau between $n = 4$ and $n = 5$, with the $n = 6$ adducts predicted to be even less stable. These trends are more easily seen from the apparent CO binding energies, $\Delta E_{ads}(n)$, shown in Table 2. For the $Mo_3S_7^+(CO)_n$ adducts, the apparent CO binding energies decrease by ~0.25 eV per added CO until $n = 5$ for which the binding energy is predicted to be essentially zero. The sequential CO binding energies for $W_3S_7^+(CO)_n$

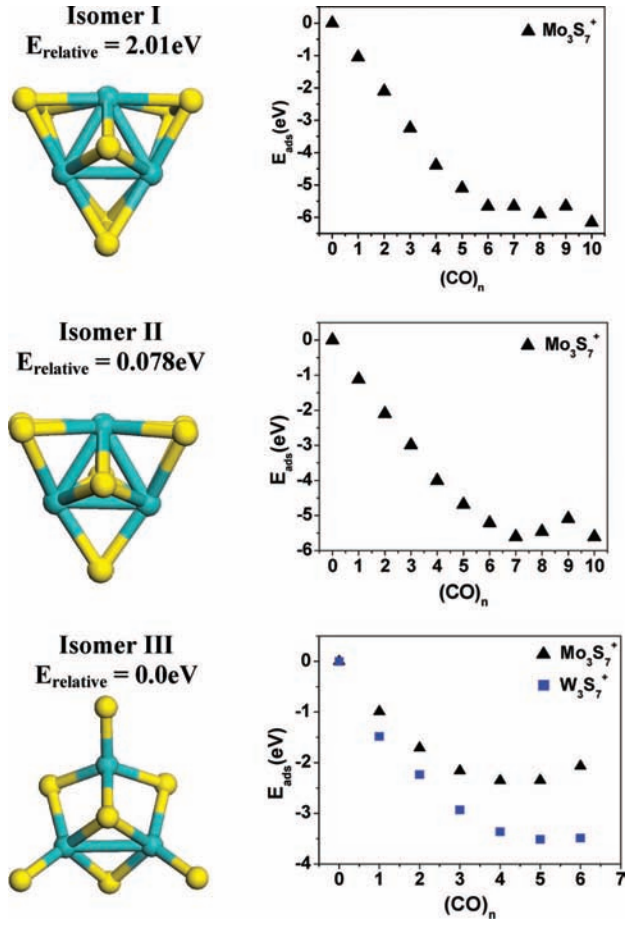

Figure 6. Optimized structures for the three lowest energy isomers of the $M_3S_7^+$ (M = Mo, W) cluster. Figures adjacent to each isomer show the total adsorption energies for sequential adsorption of CO molecules to the $M_3S_7^+$ clusters as determined by DFT calculations.

TABLE 2: Calculated Binding Energies, $\Delta E_{ads}(n)$, for the Consecutive Addition of *n*CO Molecules to Isomer III of the $M_3S_7^+$ Cluster (M = Mo, W)[a]

n	$\Delta E_{ads}(n)$ $Mo_3S_7(CO)_n^+$	$\Delta E_{ads}(n)$ $W_3S_7(CO)_n^+$
1	−0.99	−1.48
2	−0.72	−0.75
3	−0.46	−0.70
4	−0.19	−0.43
5	+0.006	−0.15**
6	+0.28	+0.026

[a] All energies are given in eV. **Denotes breakage in the adduct cluster.

exhibit a somewhat different behavior, with a large drop in apparent binding energy between the first ($n = 1$) and second ($n = 2$) CO addition, whereas the second ($n = 2$) and third ($n = 3$) additions have nearly the same binding energy. Beyond $n = 3$, the apparent CO binding energies for the W adducts steadily decrease and eventually becomes positive for $n = 6$.

On the basis of the calculated trends in consecutive CO binding energies, we would expect to observe the $n = 4$ adducts for isomer III for both the Mo and the W clusters. In fact, the $n = 4$ adduct is observed as a small peak in the $Mo_3S_7^+(CO)_n$ mass spectrum, but not in the product mass spectrum for the W cluster (see Figure 5). As was previously found for the $M_2S_6^+(CO)_3$ adducts, the probability of observing the $n = 4$ adduct depends on the cluster's stability with respect to fragmentation when the metal atoms bind to more than one CO

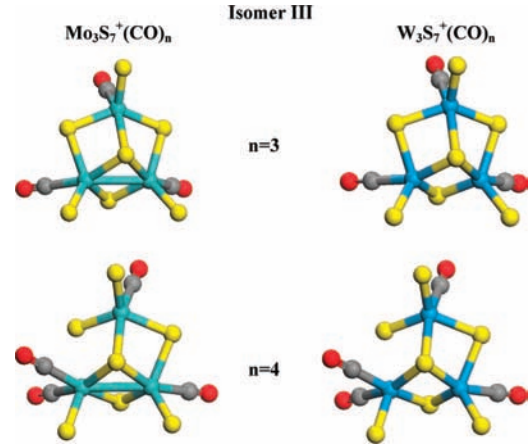

Figure 7. Geometry-optimized structure of the $n = 3$ and $n = 4$ CO adducts of isomer III of the $M_3S_7^+$ (M = Mo, W) clusters as determined from DFT calculations.

molecule. The optimized structures for the $n = 3$ and $n = 4$ CO adducts are shown in Figure 7. For both Mo and W, addition of the fourth CO causes a M−S−M bridge bond to break. On the basis of the mass spectra in Figure 5, it would appear that the $n = 4$ adduct survives on the time scale of detection for the Mo cluster but not for the W cluster. According to the DFT optimization results (not shown), when a fifth CO molecule is added to the $W_3S_7^+(CO)_4$ adduct, it undergoes fragmentation into a $WS_3(CO)$ and $W_2S_4^+(CO)_4$ species. Although the latter behavior may be an isolated case, the DFT calculations support the idea that the smaller clusters become structurally unstable when the number of bonded CO molecules exceeds the number of metal atoms, even though the total CO adsorption energy may continue to increase.

Overall, the predicted trends in CO adsorption energies and adduct stability for isomer III are more consistent with the observed product mass spectra than that for isomers I and II for both the Mo and the W clusters. Therefore, we assign the structure of the $M_3S_7^+$ cluster to that of isomer III (Figure 6).

$M_5S_7^+$ Cluster. The product distributions for the $M_5S_7^+$ clusters interacting with CO are shown in Figure 8. For both Mo and W, the observed products correspond to $M_5S_7^+(CO)_n$ adducts up to $n = 6$, with no higher mass products detected. The $n = 5$ adduct is the most probable for both the Mo and the W clusters, although the $n = 6$ adduct peak for the Mo cluster has nearly the same intensity. Although these clusters have only five metal atoms, the high probability for $n = 6$ suggests that they behave differently toward CO binding than do the smaller clusters discussed above.

Figure 9 shows the two lowest energy isomer structures for the $M_5S_7^+$ cluster. Two other higher energy structures were also considered ($E_{relative} \geq 1$ eV), but are not presented because their predicted CO adsorption energy trends were also inconsistent with the observed CO adduct product yields. The higher energy structure, isomer I, consists of a trigonal bipyramidal arrangement of the five metal atoms with an overall cluster symmetry of C_{2v} (C_2 axis perpendicular to page in Figure 9). This structure maximizes the number of bridge bonded sulfur atoms and results in three sets of inequivalent metal atom sites, that is, at the poles of the bipyramid, and two distinguishable sites in the equatorial plane. The lowest energy structure, isomer II, has as its core the tetrahedral Mo_4S_6 cluster whose compact cage structure has been shown to be especially stable as both an anion[20] and a cation.[21] The fifth Mo atom is attached at the base of the tetrahedron via three sulfur bridge bonds and is capped by a

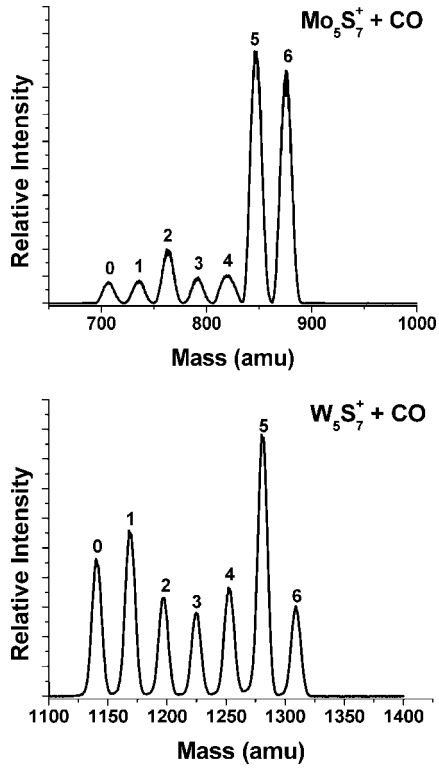

Figure 8. Mass spectra of products formed from collisions of the $M_5S_7^+$ (M = Mo, W) cluster with a 25% CO/He gas mixture.

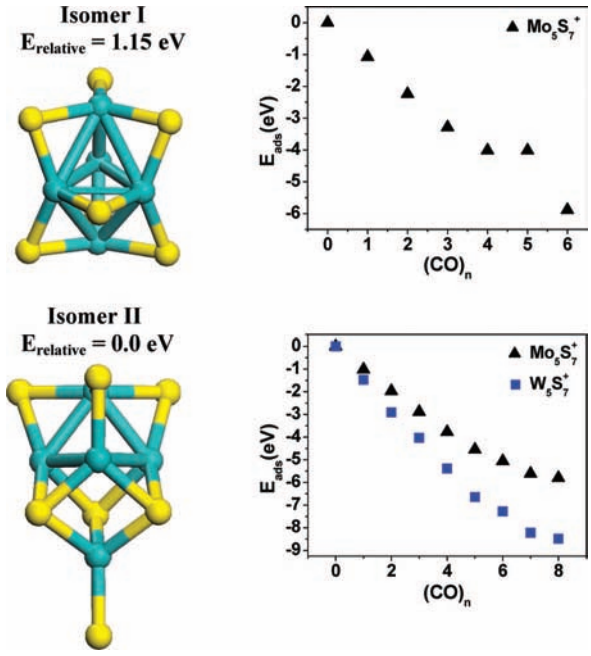

Figure 9. Optimized structures for the two lowest energy isomers of the $M_5S_7^+$ clusters (M = Mo, W). Figures adjacent to each isomer show the total adsorption energies for sequential adsorption of CO molecules to the $M_5S_7^+$ clusters as determined by DFT calculations.

triply bonded sulfur atom. Having no direct metal bonds, the fifth metal atom is more akin to the metal sites in the smaller $M_2S_6^+$ and $M_3S_7^+$ cluster. Isomer II has near C_s symmetry with the reflection plane bisecting the cluster perpendicular to the page (see Figure 9).

Also shown in Figure 9 are the calculated total adsorption energy plots for the sequential binding of CO to $Mo_5S_7^+$. For isomer I, the calculated total adsorption energy exhibits almost a linear increase up to $n = 5$, where it abruptly levels off with

TABLE 3: Calculated Binding Energies, $\Delta E_{ads}(n)$, for the Consecutive Addition of nCO Molecules to Isomer II of the $M_5S_7^+$ Cluster (M = Mo, W)[a]

n	$\Delta E_{ads}(n)$ $Mo_5S_7(CO)_n^+$	$\Delta E_{ads}(n)$ $W_5S_7(CO)_n^+$
1	−1.02	−1.48
2	−0.95	−1.43
3	−0.92	−1.12
4	−0.88	−1.35
5	−0.78	−1.26
6	−0.52	−0.63
7	−0.56	−0.94
8	−0.18	−0.26

[a] All energies are given in eV.

a relative CO binding energy close to zero ($\Delta E_{ads}(5) \approx -0.03$ eV). This calculated trend in CO adsorption energies would predict that the $Mo_5S_7^+(CO)_n$ product mass spectrum would terminate at $n = 4$, whereas the experiments show that both $n = 5$ and $n = 6$ adducts are prominent products. Note that in adding a sixth CO molecule, the total adsorption energy increases sharply by ~2 eV. This adsorption behavior is reminiscent of the increase in adsorption energy between the $n = 2$ and $n = 3$ adducts of $Mo_2S_6^+(CO)_n$, which undergo internal bond breaking with the addition of the third CO molecule (see Figures 3 and 4). Indeed, the DFT calculations predict that the addition of a sixth CO molecule to isomer I leads to Mo−Mo bond breaking in the triangular metal core (not shown). Despite the high CO adsorption energy or ultimate fate with respect to dissociation, the probability for forming the $n = 6$ adduct of isomer I is small due to the low total adsorption energy of the $n = 5$ adduct, which acts as its precursor in sequential addition. The predicted absence of the $n = 5$ adducts disagrees with the observed product mass spectrum (Figure 8); hence, isomer I is unlikely to be the correct structure of the $Mo_5S_7^+$ cluster.

The total CO adsorption energies for isomer II of the $M_5S_7^+$ cluster exhibit an almost linear gain with sequential CO addition up to $n = 5$, beyond which the adsorption energy begins to level off at $n = 8$ (see Figure 9; Table 3). The latter would predict adduct formation beyond what is observed experimentally ($n > 6$), but a more complete picture of adduct stability comes from consideration of the adduct structures. Figure 10 shows the calculated structures of the $n = 5$ to $n = 7$ adducts for isomer II of both Mo and W. It is clearly seen that the $M_5S_7^+$ core of the $n = 6$ adduct is significantly distorted from that of the bare cluster (see Figure 9) with two CO molecules bound to one of the equatorial metal atoms. The ability to accommodate two CO molecules on one metal site is attributed to the metallic nature of the four metal atoms forming the inner tetrahedron. As seen in Figure 10, the seventh CO molecule preferentially binds to the metal atom that is separated from the M_4 tetrahedral core by three sulfur bridge bonds. Binding of CO at this metal site, however, leads to breaking two of the sulfur bridge bonds, with the $MoS(CO)_2$ fragment tethered to the larger $Mo_4S_6^+(CO)_5$ core of the cluster through the remaining bridge bonded sulfur atom. The observation of the internally fractured $n = 7$ cluster adduct will depend on its stability against further fragmentation on the time scale of our detection measurements. In this case, the dissociation of the $n = 7$ adduct into two smaller fragments may be energetically driven by the high stability of the "magic cluster" fragment, $Mo_4S_6^+(CO)_n$.[21] Dissociation would lead to cation species whose mass would fall outside the range of the intact cluster adducts in Figure 8 and were not detected. Hence, the calculated CO adsorption energetics for isomer II favor adduct formation for $n = 1-6$, but larger adducts may be subject

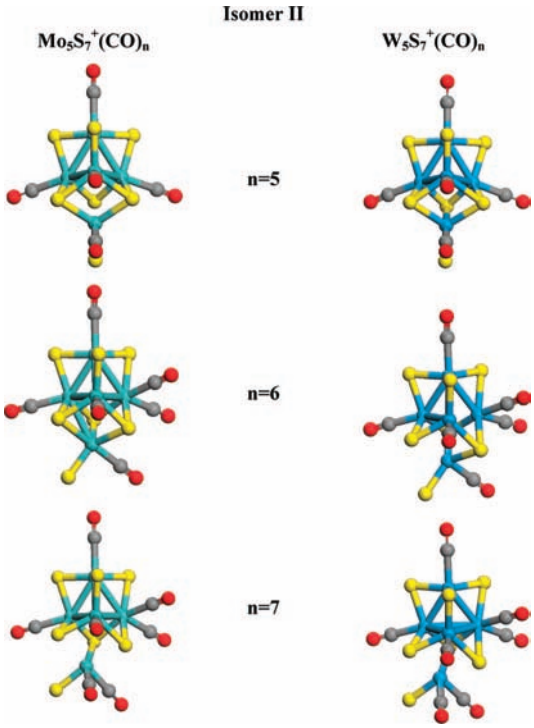

Figure 10. Geometry-optimized structure of the $n = 5-7$ CO adducts of isomer II of the $M_5S_7^+$ (M = Mo, W) clusters as determined from DFT calculations.

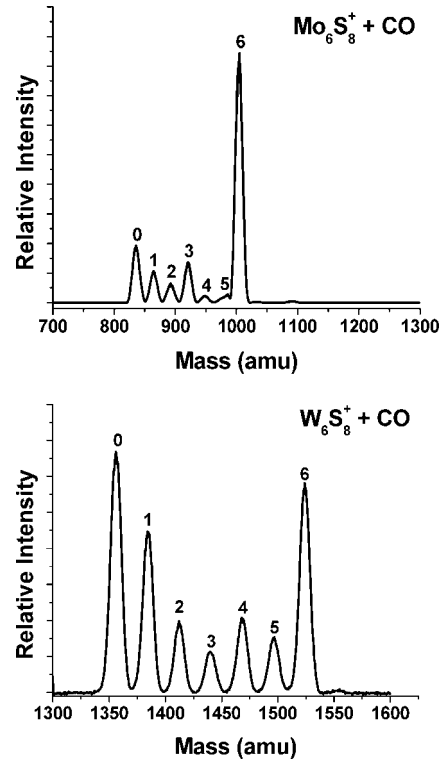

Figure 11. Mass spectra of products formed from collisions of the $M_6S_8^+$ (M = Mo, W) cluster with a 25% CO/He gas mixture.

to cluster fragmentation and dissociation. This overall picture for isomer II for both Mo and W is consistent with the observed product mass spectra that sharply terminate at the $n = 6$ adduct. Hence, we tentatively assign the structure of the $M_5S_7^+$ cluster cation to that of isomer II.

$M_6S_8^+$ Cluster. The product mass spectra resulting from interactions between the $M_6S_8^+$ (Mo and W) clusters and CO are shown in Figure 11. In the case of Mo, the $n = 6$ adduct is clearly the most favored product with only very small peaks at higher mass corresponding to CO adducts with $n = 7-9$. The CO adduct distribution for the W cluster also shows a maximum at $n = 6$; however, the mass peaks corresponding to the bare cluster ion and the $n = 1$ CO adduct are of comparable intensity. A very small peak corresponding to the $n = 7$ adduct is also observed. The fact that the product mass spectra for both Mo and W exhibit a high probability for the $n = 6$ adduct is consistent with the qualitative expectation of one CO molecule bound on each of the six metal atoms of the $M_6S_8^+$ cluster.

Figure 12 shows the calculated lowest energy structures for the $Mo_6S_8^+$ cluster (the $W_6S_8^+$ cluster is structurally similar) as well as the calculated total adsorption energies for sequential CO addition to both the Mo and the W clusters. The highly symmetric structure of isomer I has been previously identified as the building block of the well-known Chevrel phase of molybdenum sulfide in $A_xMo_6S_8$ or $ABMo_6S_8$ solid-state compounds.[14,49] The metal atoms of isomer I are arranged to form an inner octahedron with the sulfur atoms symmetrically placed in the triangular faces (near O_h symmetry).

Because the Mo_6S_8 moiety is known to have the "Chevrel" structure of isomer I in solid-state and solution-phase chemistry, it was expected that the calculated CO adsorption energies of isomer I would follow the experimentally observed CO adduct product distributions. In fact, the calculated total CO adsorption energies for Mo and W (see Figure 12) suggest that adducts with more than six CO molecules should be observable, whereas the experimental mass spectra show that adducts with $n > 6$

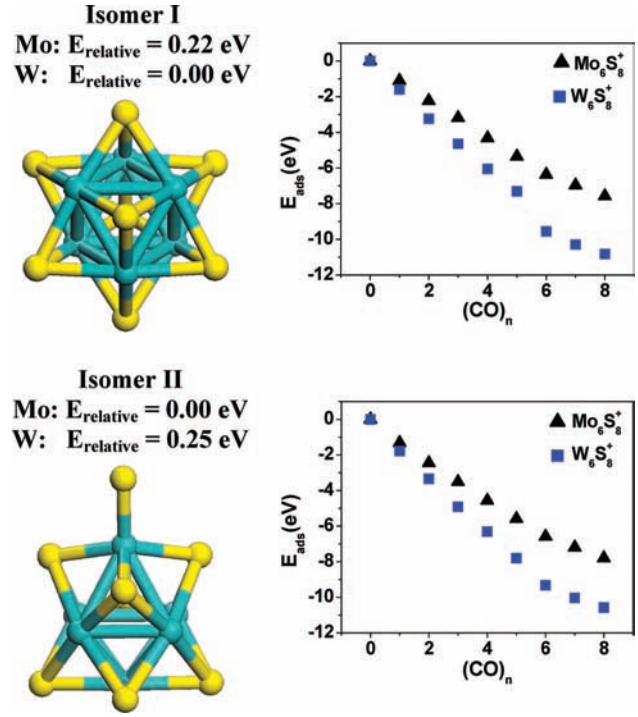

Figure 12. Optimized structures of the two lowest energy isomers of the $M_6S_8^+$ (M = Mo, W) clusters. Figures adjacent to each isomer show the total adsorption energies for sequential adsorption of CO molecules to the $M_6S_8^+$ clusters as determined by DFT calculations.

have very low probability. The theoretical result is perhaps not too surprising, as the $M_5S_7^+$ cluster with a similar metal internal framework was also predicted to bind more than one CO per metal atom. Nonetheless, the calculations for isomer I show a significant decrease in the binding energy for placing two CO molecules onto a single metal site. Specifically, the decrease in apparent CO binding energy between the $n = 6$ and $n = 7$

TABLE 4: Calculated Binding Energies, $\Delta E_{ads}(n)$, for the Consecutive Addition of nCO Molecules to the $M_6S_8^+$ Cluster (M = Mo, W)[a]

	$\Delta E_{ads}(n)$ $Mo_6S_8(CO)_n^+$		$\Delta E_{ads}(n)$ $W_6S_8(CO)_n^+$	
n	isomer I	isomer II	isomer I	isomer II
1	−1.32	−1.10	−1.78	−1.60
2	−1.14	−1.12	−1.55	−1.64
3	−1.06	−0.96	−1.57	−1.40
4	−1.04	−0.95	−1.45	−1.41
5	−1.03	−0.86	−1.50	−1.26
6	−1.00	−1.38	−1.52	−2.24
7	−0.60	−0.60	−0.72	−0.73
8	−0.60	−0.60	−0.54	−0.54

[a] All energies are given in eV.

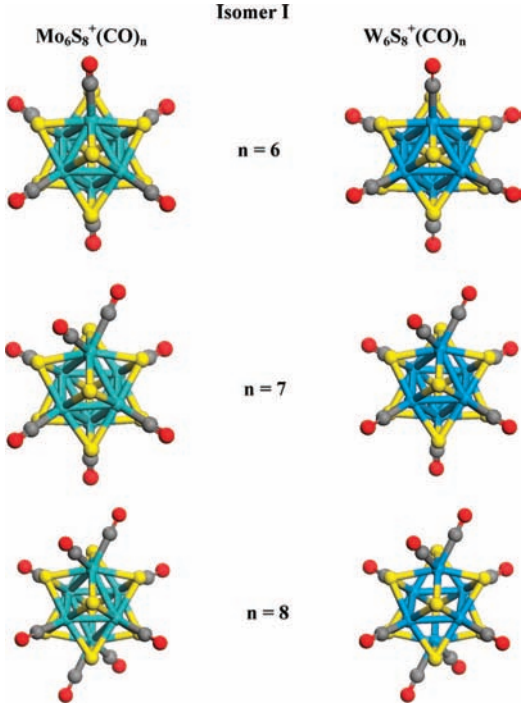

Figure 13. Geometry-optimized structures for the $n = 6-8$ CO adducts of isomer I of the $M_6S_8^+$ (M = Mo, W) clusters as determined from DFT calculations.

adducts is 40% for Mo and 53% for W (see Table 4). The latter can be qualitatively understood by inspecting the optimized structures for the $n = 6$, 7, and 8 adducts shown in Figure 13. Relative to the $n = 6$ adduct, it is seen that the addition of a second CO molecule to a single metal atom site introduces strain into the cluster framework as well as reorientation of the nearby CO molecules to minimize repulsive interactions. As a result, the gain in energy resulting from binding additional CO molecules is offset by the strain and CO crowding introduced into the adduct structure. The balance between these two effects will determine the overall stability of the adduct, and the current calculations for isomer I yield the correct trends for the relative adduct stabilities, but appear to overestimate the CO binding energies of the larger adducts ($n > 6$).

In searching for other low energy isomers of $M_6S_8^+$, a geometry optimization was performed in which the beginning structure was that of a bulk MS_2 reduced to the proper stoichiometry. The resulting structure, isomer II (Figure 12), has a calculated total energy that is lower than isomer I for the Mo cluster (−0.22 eV) and higher than isomer I for the W cluster (+0.25 eV). The prediction of different lowest energy

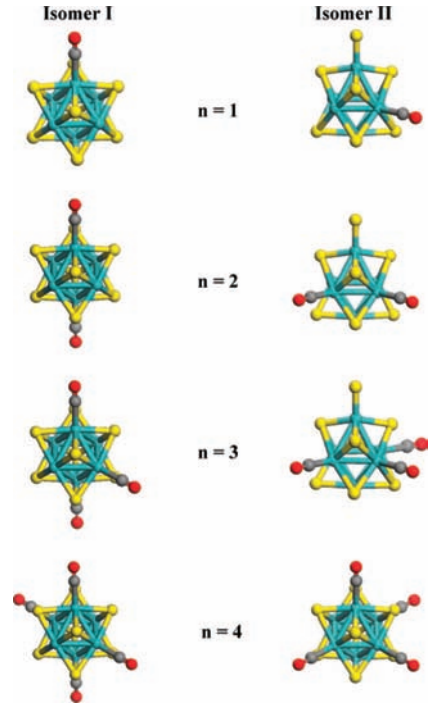

Figure 14. Comparison of the geometry-optimized structures for CO adducts ($n = 1-4$) of isomers I and II of the $Mo_6S_8^+$ cluster as determined from DFT calculations.

structures for the Mo and W clusters is unique among the small clusters studied in this work. The structure of isomer II is similar to isomer I except that two of the face centered sulfur atoms have moved to form a Mo−S−Mo bridge bond on one edge of the base of metal octahedron and a Mo−S dangling bond with one of the metal atoms at the apex of the metal octahedron. These structural changes lower the symmetry of the cluster to C_s, but the metal atoms retain an octahedral configuration.

From Figure 12 and Table 4, it is seen that the trends in calculated total CO adsorption energies for isomer II are very similar to that for isomer I for both Mo and W. Moreover, the calculated CO binding energies for the $n = 7$ and $n = 8$ adducts are essentially identical for both isomer I and isomer II (see Table 4). The latter can be explained by inspection of the optimized CO adduct structures as shown for the $n = 1-4$ adducts of the $Mo_6S_8^+$ cluster in Figure 14. For $n = 1-3$, the CO adducts of isomers I and II retain their distinct structures. For $n = 4$, however, the geometry optimization procedure results in isomer II rearranging to form an $n = 4$ adduct of isomer I. It is also seen that the $n = 4$ adduct resulting from rearrangement of isomer II has one of the CO molecules in a position different from that of the calculated lowest energy structure for the $n = 4$ adduct of isomer I. As shown in Table 4, this difference in CO binding arrangement leads to somewhat different sequential CO binding energies for the $n = 5$ and $n = 6$ adducts. The differences in total energies for the adducts of isomer I and isomer II with $n > 4$, however, are relatively small (≤0.02 eV), and so these different CO addition pathways are probably indistinguishable under experimental conditions. Beyond $n = 6$, where all of the metal atom sites are occupied by one CO molecule, the cluster adducts formed by either isomeric pathway are structurally identical and so are the $n = 7$ and $n = 8$ total adsorption energies. The calculated structures and CO adsorption trends for the $W_6S_8^+$ cluster are essentially the same as those for the $Mo_6S_8^+$ cluster discussed above.

Because of the similarities in the total energy of the CO adducts and the predicted isomer interconversion for adducts

with $n \geq 4$, the experimental product distributions cannot provide unambiguous evidence for isomer I or II as being the preferred structure for the free $M_6S_8^+$ cation cluster. Previous DFT studies have reported the existence of both isomers with binding energies only ~0.1 eV apart, with the Chevrel structure (isomer I) still being the most stable.[33] The present DFT calculation, therefore, gives a reasonable prediction of the relative isomer energies for the free $M_6S_8^+$ cation clusters. It is also possible that both isomers I and II coexist under the conditions of our cluster source or readily interconvert depending on the internal energy of the clusters. In that case, the observed adduct product distributions would reflect the CO binding of both isomers. As shown above, however, isomer I is preferred in the presence of strongly interacting adsorbates like CO. This is consistent with the Chevrel structure being the most stable in other chemically bonded environments, for example, deposited on surfaces[50,51] and in solid phases.[12,13]

Summary and Conclusions

In this work, we have used a combination of experiment and DFT to study the CO adsorption properties of several small metal sulfide clusters, $M_xS_y^+$ (M = Mo, W; x/y = 2/6, 3/7, 5/7, 6/8), as a way to probe the cluster's electronic and atomic structure. Specifically, the mass distribution of $M_xS_y^+(CO)_n$ adducts formed by collisions between the cluster cation and CO molecules is found to be very sensitive to cluster structure and provides a way to distinguish between low energy isomers predicted by theory. For the two smallest clusters, $M_2S_6^+$ and $M_3S_7^+$, the structural isomers differ by less than 0.1 eV, yet only the lowest energy structure yielded consecutive CO adsorption energies that were consistent with the experimental data. The predicted ground-state structures for the $M_2S_6^+$ and $M_3S_7^+$ clusters involve M−S−M bridge bonds as well as terminal sulfur atoms on each metal atom.

Similar comparisons of predicted CO adsorption behavior to experimental CO adduct product distributions also provide evidence for assigning the ground-state structures of the $M_5S_7^+$ and $M_6S_8^+$ clusters. The latter contain metallic cores with most of the sulfur atoms bonded along the edges or in the faces of the metal core structure. The metallic core structure of substoichiometric clusters like $M_5S_7^+$ and $M_6S_8^+$ has been attributed to partially filled d-orbitals on the metal atoms, maximizing the number of sulfur binding sites at edges and faces. The latter maximize electronic interactions between the Mo−S atoms via d−s−p orbital hybridization.[32,33]

Experimentally, the most probable $M_xS_y^+(CO)_n$ adducts observed are those with $n \leq x$, that is, a maximum of one CO molecule per metal site. As a general feature, the DFT calculations show that adding more than one CO molecule to a metal site causes considerable distortion of the cluster. In fact, the $M_2S_6^+$ and $M_3S_7^+$ (M = Mo, W) clusters are predicted to internally fragment when $n > x$, which may explain the absence of such adducts in the experimental product distributions despite having a lower total energy than the $n = x$ adduct. Similarly, the $n = 6$ and 7 adducts of $M_5S_7^+$ are predicted to be more stable than the $n = x = 5$ adduct, but only the $n = 6$ adduct is observed experimentally. The DFT calculations provide a possible explanation by showing that the $n = 7$ adduct undergoes internal bond breaking whereas the $n = 6$ framework is stable, albeit highly distorted. For the $M_6S_8^+$ cluster, the calculations predict that the two lowest energy isomers can bind to more than six CO molecules without fragmentation, although the apparent binding energy drops significantly for adducts with $n > 6$. The ability to bind additional CO molecules is likely a reflection of the metallic nature of the M_6 core of the $M_6S_8^+$ cluster. Interestingly, the DFT calculations also show that the addition of four CO molecules to the $M_6S_8^+$ cluster can lead to isomerization of the lower symmetry isomer to the more symmetric "Chevrel" isomer.

Finally, we note that the calculated adsorption energies for the first CO molecule onto the $M_xS_y^+$ cluster cations with x = 2, 3, and 5 are very similar, with a value of ~1 eV for the Mo clusters and ~1.5 eV for the W clusters. Essentially, the same adsorption energies were obtained in our earlier study of CO addition to the $Mo_4S_6^+$ and $W_4S_6^+$ "magic" clusters (M = Mo, W).[21] The $M_6S_8^+$ "Chevrel" clusters studied here show somewhat higher CO binding energies for both Mo (1.3 eV) and W (1.8 eV). These values can be compared to previous studies of CO bonding, which have focused on larger two-dimensional clusters (platelets) whose structures mimic bulk MoS_2.[27,28] Binding of CO only occurs at the edges of the platelets, which can be either Mo or S terminated. These 2D clusters are used as models for the active catalytic species in hydrotreating catalysts, which are composed of small nanoplatelets of near-stoichiometric MoS_2. In their study of $Mo_{28}S_x$ (x = 48, 60, 84), Zeng et al. obtained a first CO binding energy of 1.2 eV at 4-coordinated and ~0.5 eV for 6-coordinated Mo edge sites.[28] For the near stoichiometric $Mo_{16}S_x$ (x = 29, 34, 38) clusters, the same group calculated a range of 1.1−1.3 eV for the first CO binding energies at 4-coordinated Mo edge sites (depending on exact geometry of metal site).[27] Near additivity of adsorption energy is also observed for multiple CO additions on the large clusters, similar to what is predicted for the smaller $Mo_4S_6^+$, $Mo_5S_7^+$, and $Mo_6S_8^+$ clusters in this work. Despite the large variation in structure, the first CO bonding energies are remarkably similar between these larger bulk-like clusters and the small clusters studied here, even though the $Mo_4S_6^+$, $Mo_5S_7^+$, and $Mo_6S_8^+$ have metallic cores that are absent in bulk MoS_2. These results suggest that the metal−CO interaction is highly localized with the detailed structure of the surrounding cluster playing only a minor role. Because CO is known to bind to the same metal sites that are also active for catalysis, it is likely that even the smaller clusters 3D clusters are active for promoting surface reactions. In particular, the high CO adsorption energies and high number of active sites (6) per unit volume make the $Mo_6S_8^+$ "Chevrel" cluster an interesting candidate as a supported nanocatalyst. Indeed, recent DFT calculations by Seifert et al. have explored the binding of the Mo_6S_8 clusters on a Au(111) surface and have shown it to strongly bind to the Au surface with only minor structural changes.[50,51] We are currently exploring the reactivity of the Mo_6S_8 cluster deposited on a Au(111) surface using mass-selected deposition as recently demonstrated for the Mo_4S_6/Au(111) system.[35]

Acknowledgment. We wish to thank Dr. Ping Liu and Dr. James Muckerman, Brookhaven National Laboratory, for helpful discussions and guidance with the DFT calculations. This research was carried out at Brookhaven National Laboratory under contract DE-AC02-98CH10086 with the U.S. Department of Energy (Division of Chemical Sciences).

References and Notes

(1) Tenne, R.; Rao, C. N. R. *Philos. Trans.* **2004**, *362*, 2099.
(2) Tenne, R. *Chem.-Eur. J.* **2002**, *8*, 5296.
(3) Tenne, R. *Colloids Surf.* **2002**, *208*, 83.
(4) Seifert, G.; Kohler, T.; Tenne, R. *J. Phys. Chem. B* **2002**, *106*, 2497.
(5) Parilla, P. A.; Dillion, A. C.; Parkinson, B. A.; Jones, K. M.; Alleman, J.; Riker, G.; Ginley, D. S.; Heben, M. J. *J. Phys. Chem. B* **2004**, *108*, 6197.

(6) Enyashin, A. N.; Gemming, S.; Bar-Sada, M.; Popovitz-Biro, R.; Hong, S. Y.; Prior, Y.; Tenne, R.; Sieffert, G. *Angew. Chem., Int. Ed.* **2007**, *46*, 623.
(7) Rapoport, L.; Bilik, Y.; Feldman, Y.; Homyonfer, M.; Cohen, S. R.; Tenne, R. *Nature* **1997**, *387*, 791.
(8) Thurston, T. R.; Wilcoxon, J. P. *J. Phys. Chem. B* **1998**, *103*, 11.
(9) Chhowalla, M.; Amaratunga, G. A. J. *Nature* **2000**, *407*, 164.
(10) Chen, J.; Wu, F. *Appl. Phys., A: Mater. Sci. Process.* **2004**, *78*, 989.
(11) Topsoe, H.; Clausen, B. S.; Massoth, F. E. *Hydrotreating Catalysts: Catalysis-Science and Technology*; Springer-Verlag: Berlin-Heidelberg, 1996; Vol. 11.
(12) Umarji, A. M.; Rao, G. V. S.; Janawadkar, M. P.; Radhakrishnan, T. S. *J. Phys. Chem. Solids* **1980**, *41*, 421.
(13) Mancour-Billah, A.; Chevrel, R. *J. Solid State Chem.* **2003**, *170*, 281.
(14) Paskach, T. J.; Schrader, G. L.; McCarley, R. E. *J. Catal.* **2002**, *211*, 285.
(15) Dance, I. G.; Fischer, K. J.; Willett, G. D. *J. Chem. Soc., Dalton Trans.* **1997**, 2557.
(16) Nakat, J. H. E.; Dance, I. G.; Fischer, K. J.; Rice, D.; Willett, G. D. *J. Am. Chem. Soc.* **1991**, *113*, 5141.
(17) Dance, I. G. *Chem. Commun.* **1998**, 523.
(18) Zhang, N.; Yu, Z.; Wu, X.; Gao, Z.; Zhu, Q.; Kong, F. *J. Chem. Soc., Faraday Trans.* **1993**, *89*, 1779.
(19) Lightstone, J. M.; Mann, H. A.; Wu, M.; Johnson, P. M.; White, M. G. *J. Phys. Chem. B* **2003**, *107*, 10359.
(20) Bertram, N.; Kim, Y. D.; Gantefor, G.; Sun, Q.; Jena, P.; Tamuliene, J.; Seifert, G. *Chem. Phys. Lett.* **2004**, *396*, 341.
(21) Lightstone, J. M.; Patterson, M. J.; White, M. G. *Chem. Phys. Lett.* **2005**, *413*, 429.
(22) Nakat, J. E.; Fisher, K. J.; Dance, I. G.; Willet, G. D. *Inorg. Chem.* **1993**, *32*, 1931.
(23) Dance, I. G.; Fisher, K. J.; Willett, G. D. *Inorg. Chem.* **1996**, *35*, 4177.
(24) Brandle, M.; Calzaferri, G.; Lanz, M. *Chem. Phys.* **1995**, *201*, 141.
(25) Orita, H.; Uchida, K.; Itoh, N. *J. Mol Catal. A: Chem.* **2003**, *193*, 197.
(26) Orita, H.; Uchida, K.; Itoh, N. *Appl. Catal., A* **2004**, *258*, 115.
(27) Zeng, T.; Wen, X.-D.; Wu, G.-S.; Li, Y.-W.; Jiao, H. *J. Phys. Chem. B* **2005**, *109*, 2846.
(28) Zeng, T.; Wen, X.-D.; Li, Y.-W.; Jiao, H. *J. Phys. Chem. B* **2005**, *109*, 13704.
(29) Travert, A.; Dujardin, C.; Mauge, F.; Cristol, S.; Paul, J. F.; Payen, E.; Bougeard, D. *Catal. Today* **2001**, *70*, 255.
(30) Siefert, G.; Taluliene, J.; Gemming, S. *Comput. Mater. Sci.* **2006**, *35*, 316.
(31) Gemming, S.; Tamuliene, J.; Seifert, G.; Bertram, N.; Kim, Y. D.; Gantefor, G. *Appl. Phys., A* **2005**, ???
(32) Murugan, P.; Kumar, V.; Kawazoe, Y.; Ota, N. *Phys. Rev. A: At., Mol., Opt. Phys.* **2005**, *71*, 063203.
(33) Murugan, P.; Kumar, V.; Kawazoe, Y.; Ota, N. *J. Phys. Chem. A* **2007**, *111*, 2778.
(34) Seifert, G.; Tamuliene, J.; Gemming, S. *Comput. Mater. Sci.* **2006**, *35*, 316.
(35) Lightstone, J. M.; Patterson, M. J.; Liu, P. J. C.; Lofaro, J.; White, M. G. *J. Phys. Chem. C* **2008**, *112*, 11495.
(36) Gemming, S.; Seifert, G. *AIP Conf. Proc.* **2005**, *786*, 353.
(37) Lauritsen, J. V.; Kibsgaard, J.; Helvig, S.; Topsoe, H.; Clausen, B. S.; Laegsgaard, E.; Besenbacher, F. *Nat. Nanotechnol.* **2007**, *2*, 53.
(38) Lightstone, J. M.; Patterson, M.; White, M. G. *J. Phys. Chem. A* **2006**, *110*, 3505.
(39) Koelling, D. D.; Harmon, B. N. *J. Phys. Chem. Solids* **1977**, *10*, 3107.
(40) He, S.-G.; Xie, Y.; Guo, Y.; Bernstein, E. *J. Chem. Phys.* **2007**, *126*, 194315.
(41) Hadjikyriacou, A. I.; Coucouvanis, D. *Inorg. Chem.* **1987**, *26*, 2400.
(42) Hibble, S. J.; Feaviour, M. R.; Almond, M. J. *J. Chem. Soc., Dalton Trans.* **2001**, 935.
(43) Llusar, R.; Uriel, S.; Vicent, C.; Clemente-Juan, J. M.; Coronado, E.; Gomez-Garcia, C. J.; Braida, B.; Canadell, E. *J. Am. Chem. Soc.* **2004**, *126*, 12076.
(44) Muller, A.; Sarkar, S.; Bhattacharyya, R. G.; Pohl, S.; Dartman, M. *Angew. Chem., Int. Ed. Engl.* **1978**, *17*, 535.
(45) Guo, B. C.; Kerns, K. P.; Castleman, A. W. *J. Chem. Phys.* **1992**, *96*, 8177.
(46) Vajda, S.; Leisner, T.; Wolf, S.; Woste, L. H. *Philos. Mag. B* **1999**, *79*, 1353.
(47) Vajda, S.; Wolf, S.; Leisner, T.; Busolt, U.; Woste, L. H.; Wales, D. J. *J. Chem. Phys.* **1997**, *107*, 3492.
(48) Davidson, E. R.; Kunze, K. L.; Machado, F. B. C.; Chakravorty, S. J. *Acc. Chem. Res.* **1993**, *26*, 628.
(49) Paskach, T. J.; Hilsenbeck, S. J.; Thompson, R. K.; McCarley, R. E.; Schrader, G. L. *J. Alloys Compd.* **2000**, *311*, 169.
(50) Popov, I.; Gemming, S.; Seifert, G. *Phys. Rev. B* **2007**, *75*, 245436.
(51) Popov, I.; Kunze, T.; Gemming, S.; Seifert, G. *Eur. Phys. J. D* **2007**, *45*, 439.

JP807318C